13

Influence of Ba atom adsorption and implantation of Ba^+ ions on the electronic structure of single crystalline Ge

© D.A. Tashmukhamedova,[1] B.E. Umirzakov,[1] Y.S. Ergashov,[1] M.B. Yusupjanova,[1] R.M. Yorkulov[1]

[1] Tashkent State Technical University, Tashkent, Uzbekistan
[2] Arifov Institute of Ion-Plasma and Laser Technologies, Uzbekistan Academy of Sciences
100125 Tashkent, Uzbekistan
e-mail: ftmet@mail.ru

Received August 5, 2021
Revised December 24, 2021
Accepted December 27, 2021

The effect of the adsorption of Ba atoms with a thickness of $\theta \leq 3-4$ monolayers and the implantation of Ba^+ ions with an energy of $E_0 = 0.5-2$ keV on the density of states of electrons in the valence band, the parameters of the energy bands, and the emission and optical properties of Ge(111) has been studied for the first time. It is shown that during the adsorption of Ba atoms with $\theta = 1$ monolayer, the value of the thermoelectric work function φ decreases by ~ 1.9 eV, and the value of the secondary electron emission coefficient and the quantum yield of photoelectrons Y increases by 1.5–2 times. In the case of implantation of Ba^+ ions with $E_0 = 0.5$ keV at an irradiation dose $D = 6 \cdot 10^{16}$ cm^{-2}, the density of state of valence electrons and the parameters of the energy bands change sharply; the quantum yield of photoelectrons increases by a factor of 2 or more. The observed changes are explained by the formation on the surface of a thin ($\sim 25-30$ Å) amorphous doped layer consisting of nanoscale phases of the Ba–Ge type ($\sim 60-65$ at.%). And excess (unbound) Ba and Ge atoms. In this case, the band gap E_g decreases by ~ 0.3 eV.

Keywords: Ion implantation, quantum yield of photoelectrons, emission efficiency, heating, band gap, amorphous layer.

DOI: 10.21883/TP.2022.04.53614.230-21

Introduction

Si, Ge, and nanostructures based on them are now used widely in various solid-state electronic devices [1–4]. Specifically, nanophases and nanolayers of metal silicides and germanides have promising applications in the design of microwave transistors and integrated circuits, and Ge_xSi_{1-x}/Si heterostructures may be used in light-emitting diodes, photodetectors, laser sources, optical and electronic instruments [5–12]. In view of this, the composition, the electronic and crystal structure, and the emission and optical properties of nanosized heterostructures and layers produced by molecular-beam, solid-phase, and vapor-phase epitaxy on the surface of Si and Ge have been studied extensively in recent years [13–16]. The method of ion implantation has been used widely in the last few years to alter the physical properties of semiconductors in a controlled change. Specifically, nanosized phases and layers of Ba, Co, Ni, Na, and Rb silicides were obtained by ion implantation in Si; their composition, electronic structure, and properties were studied; and the sizes of silicide phases at which quantum-dimensional effects appear were determined [17–23]. In the case of Ge, high-energy ($E_0 = 80$ keV) high-dose ($D = 10^{16}$ cm^{-2}) implantation of Sb, P, and As ions was used to modify the band structure [24–27].

However, no reliable theoretical and experimental data on the physical properties of nanostructures of germanides obtained by low-energy ion implantation have been presented to date.

This is the reason why the present study is aimed at examining the composition and the electronic properties of Ge(111) coated with Ba atoms and implanted with Ba^+ ions with energy $E_0 = 0.5-5$ keV.

1. Research or experimental

Single-crystalline Ge(111) p- (with a boron concentration of $\sim 5 \cdot 10^{18}$ cm^{-3}) and n-type (with a phosphorus concentration of $\sim 10^{16}$ cm^{-3}) samples $10 \times 10 \times 0.5$ mm in size were studied. On and the same experimental apparatus (type USU-2) with vacuum level $P \leq 10^{-7}$ Pa was used for thermal treatment, deposition of Ba atoms, irradiation with Ba^+ ions, Auger electron spectroscopy (AES), ultraviolet photoelectron spectroscopy (UVPS), spectroscopy of slow elastically reflected electrons (ERE), and measurement of the quantum yield of photoelectrons. The energy and the dose of Ba^+ ions were varied within the ranges of $E_0 = 0.5-5$ keV and $D = 10^{14}-10^{17}$ cm^{-2}. Prior to ion bombardment, the surface of Ge was degassed at $T = 1000$ K for 4–5 h in combination with short-term heating to $T = 1200$ K in vacuum no worse than 10^{-7} Pa.

Quantum yield of photoelectrons Y was determined at $h\nu = 10.8$ eV in accordance with the following formula: $Y = \frac{n_e}{N_{Ph}}$, where n_e is the number of photoelectrons reaching

the collector and N_{Ph} is the number of photons incident on the target surface. In the present case, $N_{Ph} = 5 \cdot 10^{14}\,s^{-1}$.

The maximum value of secondary electron emission (SEE) coefficient σ_m was determined based on the $\sigma(E_p)$ dependence.

Thermoelectric work function φ was calculated in accordance with the following formula: $\varphi = E_{Vac} - E_F$, where E_{Vac} is the vacuum level and E_F is the Fermi level. The variation of φ was determined using the Anderson method.

2. Experimental results and discussion

The UVPS spectra for p-type Ge(111) coated with a Ba film of a varying thickness deposited at room temperature are shown in Fig. 1. Binding energy E_{bind} of electrons is plotted on the abscissa; Fermi level energy E_F of germanium is determined relative to the Fermi level of pure Pd. E_v is the upper energy edge of the valence band. In what follows, the same vertical scale is set for all energy distribution curves (EDCs) of photoelectrons. This scale was chosen so that the area under the curve is proportional to the quantum yield of electrons from samples. It follows from Fig. 1 that the spectrum of pure p-type Ge(111) has well-marked features at the energies of -0.8, -1.6, -3.5, and -5.1 eV. These features are associated with the excitation of electrons from surface states (SS) and from $4p$, $4s$, and hybridized $4p + 4s$ Ge levels (Fig. 1, curve *1*).

The curves are shifted along the vertical axis for clarity. In the region of small thicknesses of the barium coating ($\theta = 0.5{-}0.6$) where electrons are still being emitted primarily from germanium, the following EDC changes are induced by an increase in θ: all Ge features become more pronounced; the start of the spectrum and peaks associated with the maxima of density of electron states in the valence band shift toward lower energies; a new peak typical of Ge emerges in the region of $E_{bind} = -6$ eV; EDCs become wider; and the quantum yield of electrons increases. The change in position of the low-energy EDC edge is apparently associated with the φ reduction, and magnitude A of the peak shift is equal to the change in band bending. The increase in Y is attributable primarily to the reduction in work function φ and the enhancement of band bending. As the barium layer thickness increases further (curves *4, 5* in Fig. 1), the intensity of germanium peaks decreases monotonically, and the structure typical of barium starts to form.

Figure 2 presents the dependences of φ, Y, and σ_m on the deposition time for the Ba$-$Ge system. The value of θ corresponding to $\varphi = \varphi_{min}$ is recognized provisionally as a single monolayer. It can be seen that the inflection point of the $\sigma_m(t)$ and $Y(t)$ dependences coincides approximately with thickness θ of a single monolayer. The values of σ_m and Y of the Ba$-$Ge system are maximized at this point. As θ increases further, the values of Y and σ_m decrease monotonically. It may be assumed that the emission

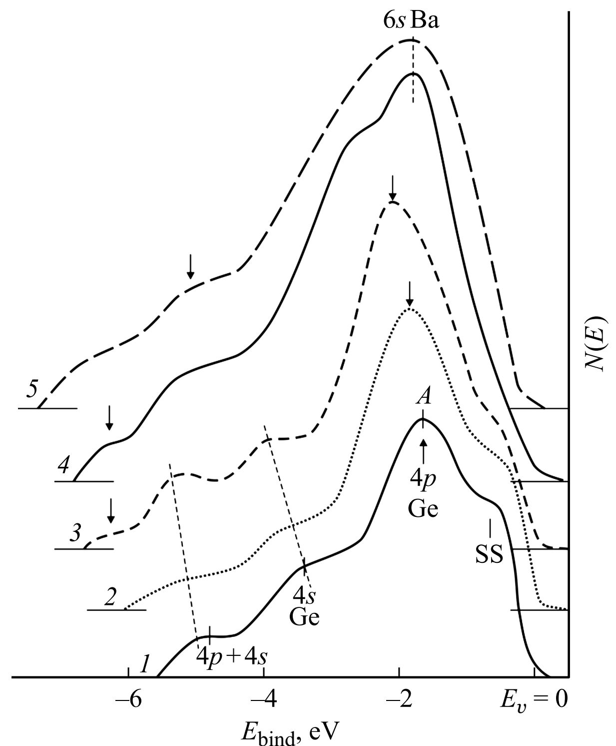

Figure 1. Ultraviolet photoelectron spectra of p-type Ge(111) with a barium film with thickness θ equal to *1* — 0, *2* — 0.2, *3* — 0.6, *4* — 1.0, and *5* — 2.0 monolayers. $h\nu = 10.8$ eV ($h\nu$ is the photon energy).

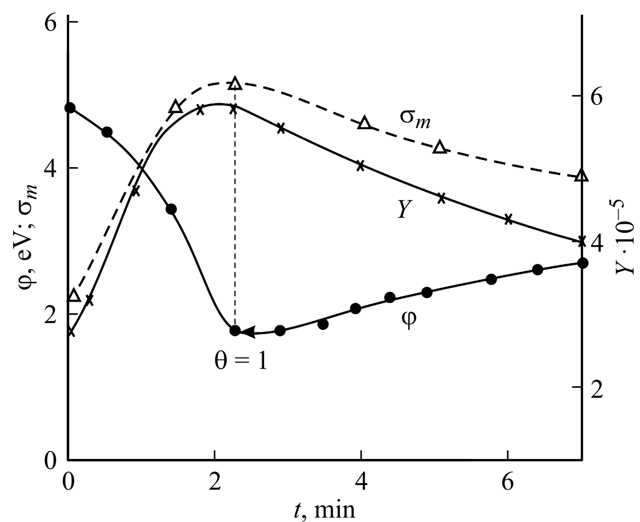

Figure 2. Dependences of φ, σ_m, and Y on the deposition time for the Ba$-$Ge(111) system.

efficiency of Ba layers is significantly lower than the one of Ge layers.

Figure 3 presents the photoelectron spectra for n-type Ge(111) implanted with Ba$^+$ ions with various doses at $E_0 = 0.5$ keV. It can be seen that the low-energy edge of the spectrum shifts toward lower binding energies

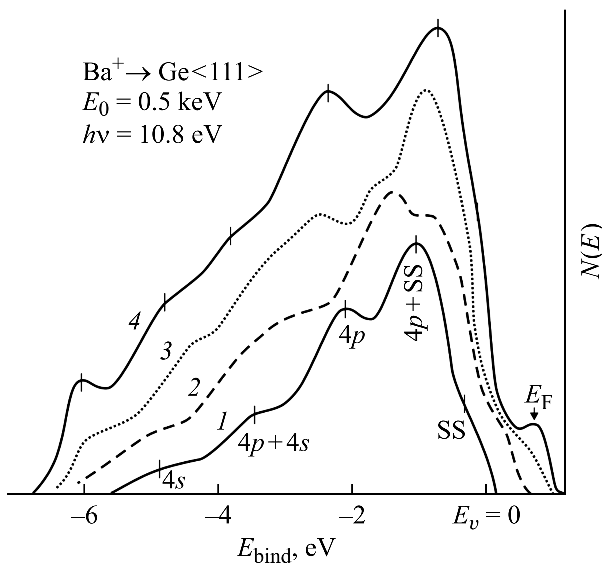

Figure 3. Ultraviolet photoelectron spectra of n-type Ge(111) implanted with Ba^+ ions with $E_0 = 0.5$ keV at dose D, cm^{-2}: *1* — 0, *2* — $2 \cdot 10^{15}$, *3* — $8 \cdot 10^{15}$, *4* — $4 \cdot 10^{16}$.

(and the high-energy edge (start) of the spectrum shifts toward higher binding energies) as the irradiation dose increases. At $D \geq 2 \cdot 10^{15}\,cm^{-2}$, a number of features typical of „high" doses emerge in the spectrum. The intensities of peaks corresponding to pure Ge decrease sharply (certain Ge peaks, including the features associated with surface states, vanish completely). As the dose increases further, new features become more intense and shift somewhat toward higher E_{bind} values. The spectra cease to change at $D = 6 \cdot 10^{16}\,cm^{-2}$; i.e., this value is saturation dose D_{sat}. At this dose, the area under the EDC (i.e., the quantum yield of photoelectrons) increases by a factor of almost two, and well-marked features at $E_{bind} = -6.1, -4.5, -3.8, -2.5, -0.7$, and $+0.6$ eV relative to the upper edge of the valence band emerge in dependence $N(E)$. The results of analysis of obtained spectra and their comparison with the spectra of germanium with a deposited barium film suggest that the observed peak at $E_{bind} = -6.1$ eV corresponds to germanium, low-intensity peaks at -4.9 and -0.2 eV correspond to unbound barium atoms, and all the other peaks are associated with barium germanides. The AES data revealed that the majority (60−70%) of barium atoms form chemical bonds with matrix atoms, producing primarily BaGe- and $BaGe_2$-type compounds. A modest-sized maximum at $E_{bind} = 0.6$ eV forms in the spectrum as a result of this.

It may be assumed that a narrow impurity band of allowed states emerges then near the lower edge of the conduction band; therefore, the width of bandgap E_g of Ge decreases sharply. The upper edge of this new band overlaps with the lower edge of the conduction band, and the properties of ion-implanted layers grow similar to the corresponding properties of metals. Unbound barium atoms are present in this case on the surface and near it. This leads to a reduction in the work function and electron affinity χ, narrowing of the band gap, and a change in E_F positions (Table 1). The values of thermoelectric φ and photoelectronic Φ work functions then become equal, and the surface layer of the examined semiconductor assumes the properties of a metal (Table 1).

Table 1. Values of the key parameters of the band structure of n-type Ge(111) implanted with various doses of Ba^+ ions with $E_0 = 0.5$ keV

Studied samples	Band parameters, eV			
	Φ, eV	φ, eV	E_g, eV	χ, eV
Ge(111)	4.9	3.5	0.7	3.4
$Ba^+ \to$ Ge(111), $E_0 = 0.5$ keV	2.4	2.4	0.4	2.4

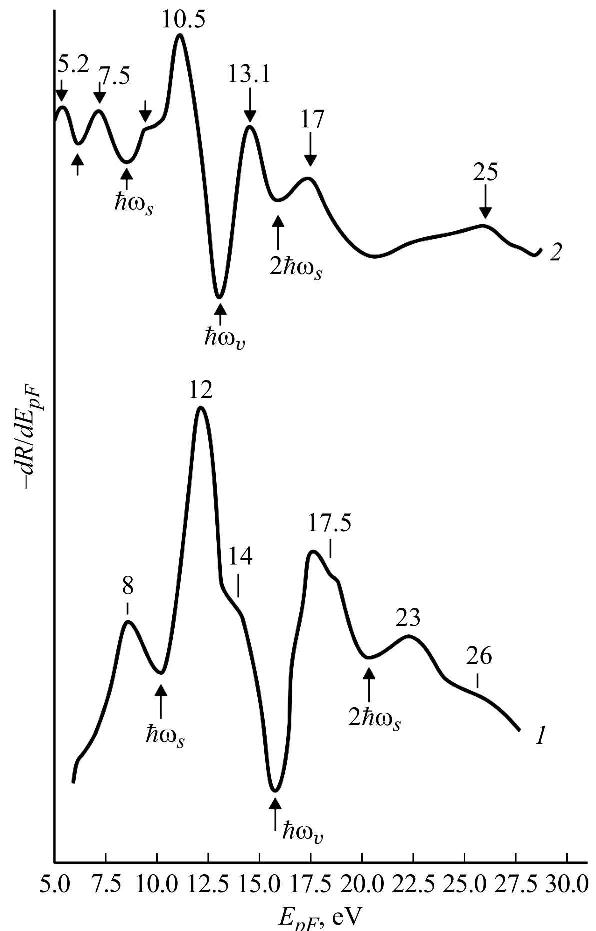

Figure 4. ERE spectra of pure n-type Ge(111) (curve *1*) and n-type Ge(111) implanted with Ba^+ ions with $E_0 = 0.5$ keV at $D = 6 \cdot 10^{16}\,cm^{-2}$ (curve *2*).

Figure 4 shows the ERE spectra within the $E_{pF} = 3{-}30$ eV range for pure n-type Ge(111) and Ge implanted with Ba^+ ions with $E_0 = 0.5$ keV at dose $D = D_{sat} = 6 \cdot 10^{16}\,cm^{-2}$, where E_{pF} is the E_p energy

Table 2. Energy position of maxima in the photoelectron and ERE spectra for Ge samples implanted with ions

Studied system	UVPS		$-dR/dE_p(E_p)$		
	E_{bind}, eV	Interpretation	E_{pF} eV	$E_{pF}-\chi$, eV	Transitions
Ge(111) p-type	-0.5	SS	5.9	2.5	SS $\to E_c^*$
	-1.3	$4p$ + SS; E_{v_1}	8.4	5	$E_{v_1}\to E_c^{**}$
	-2.1	$4s$; E_{v_2}	11.4	8	$E_{v_1}\to E_c^*$, $E_{v_3}\to E_c^{**}$
	-3.5	$4s+4p$; E_{v_5}	13.4	10	$E_{v_2}\to E^*$
	-4.8	$4s$ E_{v_4}	17.4	13	$E_{v_4}\to E^*$
			21.4	18	$E_{v_5}\to E_c^*$
Ba$^+$ $\to$ Ge(111) $E_0 = 0.5$ keV	$+0.6$	E_v^*	5.2	2.8	$E_v^*\to E_c^{**}$
	-0.7	E_{v_1}	7.5	5.1	$E_{v_2}\to E_c^{**}$
	-2.3	E_{v_2}, Ba + Ge	10.5	8.1	$E_{v_4}\to E_c^{**}$, $E_{v_5}\to E_c^*$
	-3.8	E_{v_3}	13.1	10.7	$E_{v_5}\to E_c^{**}$
	-4.5	E_{v_4}	17	14.6	$E_{v_6}\to E_{\text{vac}}$
	-6.1	E_{v_3}, $4s$ Ge	25	22.6	$E_{v_6}\to E^*$

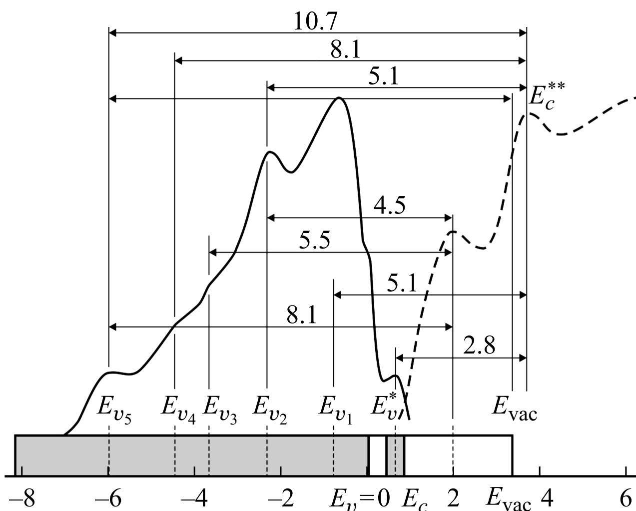

Figure 5. Energy band diagram of Ge(111) implanted with Ba$^+$ ions with $E_0 = 0.5$ keV at $D = 6\cdot 10^{16}$ cm^{-2}.

counted off from Fermi level E_F. It is known that certain minima in the $E_{pF}\le 25{-}30$ eV region are roughly coincident with the threshold energy of excitation of surface ($h\omega_s$) and bulk ($h\omega_v$) plasma oscillations and their multiples ($2h\omega_s$, $2h\omega_v$), while the positions of maxima correspond to the threshold energy of excitation of transitions between the maxima of the density of states in valence and unoccupied bands. In the case of pure Ge, maxima in the indicated E_{pF} region are observed at energies $E_{pF} = 5.9$, 8.4, 11.4, 13.4, 17.4, and 21.4 eV, and minima are found at $E_{pF} = 10.2$ ($\hbar\omega_s$), 15.6 ($\hbar\omega_v$), and 21 eV ($2\hbar\omega_s$). In the case of Ge implanted with ions, the values of $\hbar\omega_s$ and $\hbar\omega_v$ in the ERE spectrum drop to 9 and 13 eV, respectively, and a new minimum associated with the excitation of a bulk plasmon typical of barium emerges at $E_{pF} = 6$ eV. The $-dR/dE_{pF}(E_{pF})$ dependence contains primarily the maxima of compound [Ge + Ba] ($E_{pF} = 7.5$, 10, 13.5, 20, and 25 eV) and barium itself ($E_{pF} = 5$ eV).

The positions of maxima observed in EDCs of photoelectrons and curves $-dR/dE_p(E_p)$ for pure p-type Ge and Ge implanted with Ba$^+$ ions with $E_0 = 0.5$ keV at $D = 4\cdot 10^{16}$ cm^{-2} are given in Table 2. The presumed types of interband transitions of electrons with their energy estimated as $E_p = E_{pF} - e\varphi$ are also presented there.

The energy band diagram of Ge implanted with Ba$^+$ ions with $E_0 = 0.5$ keV at the saturation dose was plotted based on Figs. 3 and 4 and Table 1 (Fig. 5). It was assumed in plotting this diagram that the EDC of photoelectrons matches completely the density of states of valence electrons, and the values of interband transitions observed in the ERE spectrum are equal to the energy interval between the maxima of occupied (valence band) and unoccupied (conduction band + vacuum) states.

Conclusion

Comparative studies of the effects of deposition of Ba atoms and implantation of Ba$^+$ ions on the composition, structure, and emission properties of n- and p-type single-crystalline Ge(111) were carried out. Since the composition of surface layers does not change appreciably in the process of adsorption of Ba with $\theta\le 0.6$ monolayers, the change in electronic structure and the increase in coefficients σ_m and Y in this θ region are attributable primarily to the reduction in work function $e\varphi$ and the change in the magnitude of surface band bending. Well-marked features typical of Ba start emerging in the spectrum at $\theta = 1$ monolayer, and all Ba features become pronounced at $\theta = 2$ monolayers. The EDC of photoelectrons changes significantly upon implantation of Ba$^+$ ions with $E_0 = 0.5$ keV at doses higher than $D = 2\cdot 10^{15}$ cm^{-2}. Features typical of Ba + Ge-type compounds and excess Ba atoms emerge at $D = D_{\text{sat}} = 6\cdot 10^{16}$ cm^{-2} in the EDC. The band bending

magnitude then drops to zero. The increase in σ_m and Y under ion bombardment is more significant than the corresponding change in the case of deposition of Ba atoms with $\theta = 1$ monolayer.

Conflict of interest

The authors declare that they have no conflict of interest.

References

[1] A.S. Deryabin, A.E. Dolbak, M.Yu. Esin, V.I. Mashanov, A.I. Nikiforov, O.P. Pchelyakov, L.V. Sokolov, V.A. Timofeev. Optoelectron., Instrum. Data Process. **56** (5), 470 (2020). DOI: 10.15372/AUT20200503

[2] O.M. Sreseli, M.A. Elistratova, D.N. Goryachev, E.V. Beregulin, V.N. Nevedomskii, N.A. Bert, A.V. Ershov. Semiconductors, **54** (10), 1315 (2020). DOI: 10.1134/S1063782620100292

[3] A.V. Dvurechenskii, A.I. Yakimov, A.V. Nenashev, A.F. Zinov'eva. Phys. Solid State, **46** (1), 56 (2004).

[4] S. Wirths, R. Geiger, N. von den Driesch, G. Mussler, T. Stoica, S. Mantl, Z. Ikonic, M. Luysberg, S. Chiussi, J.M. Hartmann, H. Sigg, J. Faist, D. Buca, D. Grützmacher. Nature Photon., **9** (2), 88 (2015).

[5] G. Masini, L. Colace, G. Assanto. Mat. Sci. Eng. B, **89**, 2 (2002). DOI: 10.1016/S0921-5107(01)00781-4

[6] L. Pavesi. J. Phys. Cond. Mat., **15** (26), R1169 (2003). DOI: 10.1088/0953-8984/15/26/201

[7] Z.F. Krasil'nik, A.V. Novikov. Phys. Usp., **43**, 295 (2000). DOI: 10.1070/PU2000v043n03ABEH000703

[8] A.A. Druzhinin, I.P. Ostrovskii, Yu.N. Khoverko, S.I. Nichkalo, R.N. Koretskii. Tekhnol. Konstr. Elektron. Appar., No. 5, 19 (2012) (in Russian).

[9] I.G. Neizvestny. Optoelectron., Instrum. Data Process., **52** (5), 421 (2016). DOI: 10.15372/AUT20160501

[10] Yu.B. Bolkhovityanov, A.S. Deryabin, A.K. Gutakovskii, L.V. Sokolov. J. Cryst. Growth, **483**, 265 (2018)

[11] Sh. Saito, A.Z. Al-Attili, K. Oda, Y. Ishikawa. Semicond. Sci. Technol., **31** (4) 043002 (2016). DOI: 10.1088/0268-1242/31/4/043002

[12] J. Liu, L.C. Kimerling, J. Michel. Semicond. Sci. Tech., **27** (9), 094006 (2012). DOI: 10.1088/0268-1242/27/9/094006

[13] D.V. Yurasov, N.A. Baidakova, A.N. Yablonskiy, A.V. Novikov. Semiconductors, **54** (7), 811 (2020). DOI: 10.21883/FTP.2020.07.49511.9379

[14] A.S. Zhuravlev, S. Dickmann, L.V. Kulik, I.V. Kukushkin. Phys. Rev. B, **89** (16), 161301 (2014). DOI: 10.1103/PhysRevB.89.161301

[15] F.Yu. Solomkin, A.S. Orekhov, S.V. Novikov, N.A. Arkharova, G.N. Isachenko, N.V. Zaitseva, N.V. Sharenkova, A.U. Samunin, V.V. Klechkovskaya, A.T. Burkov. Semiconductors, **53**, 761 (2019). DOI: 10.1134/S1063782619060253

[16] L.K. Orlov, S.V. Ivin, V.M. Fomin. Tech. Phys., **62** (3), 449 (2017).

[17] B.E. Umirzakov, D.A. Tashmukhamedova, E.U. Boltaev, A.A. Dzhurakhalov. Mater. Sci. Eng. B, **101**, 124 (2003).

[18] Y.S. Ergashov, D.A. Tashmukhamedova, B.E. Umirzakov. J. Surf. Investigation: X-ray, Synchrotron and Neutron Techniques, **11** (2), 480 (2017). DOI: 10.1134/S1027451017020252

[19] R.M. Bayazitov, R.I. Batalov, E.I. Terukov, V.Kh. Kudoyarova. Phys. Solid State, **43** (9), 1633 (2001).

[20] Y.S. Ergashov, D.A. Tashmukhamedova, E. Rabbimov. J. Surf. Investigation. X-ray, Synchrotron and Neutron Techniques, *9* (2), 350 (2015). DOI: 10.1134/S1027451015020287

[21] B.E. Umirzakov, D.A. Tashmukhamedova, A.K. Tashatov, N.M. Mustafoeva. Tech. Phys., **64** (5), 708 (2019). DOI: 10.1134/S1063784219050244

[22] B. Schuller, R. Carius, S. Mantl. J. Appl. Phys., **94**, 207 (2003). DOI: 10.1063/1.1576902

[23] B.E. Umirzakov, D.A. Tashmukhamedova, D.M. Muradkabilov, K.K. Boltaev. Tech. Phys., **58** (6), 841 (2013).

[24] R. Geiger, T. Zabel, H. Sigg. Front. Mater., **2**, 52 (2015). https://doi.org/10.3389/fmats.2015.00052

[25] R.I. Batalov, R.M. Bayazitov, G.A. Novikov, V.A. Shustov, N.M. Lyadov, A.V. Novikov, P.A. Bushuikin, N.A. Baidakova, M.N. Drozdov, P.A. Yunin. Optoelectron., Instrum. Data Process., **55** (5), 423 (2019). DOI: 10.15372/AUT20190501

[26] R. Pillarisetty. Nature, **479**, 324 (2011). https://doi.org/10.1038/nature10678

[27] E. Bruno, G.G. Scapelatto, G. Bisognin. E. Carria, L. Romano, A. Carnera, F. Priolo. J. Appl. Phys, **108**, 124902 (2010). https://doi.org/10.1063/1.3520671